ARTICLE

ACS chemical biology

A Small Molecule Microarray Platform To Select RNA Internal Loop–Ligand Interactions

Jessica L. Childs-Disney, Meilan Wu, Alexei Pushechnikov, Olga Aminova, and Matthew D. Disney*

Department of Chemistry and Center of Excellence in Bioinformatics and Life Sciences, University at Buffalo, 657 Natural Sciences Complex, Buffalo, New York 14260

ABSTRACT Herein, we report the development of a microarray platform to select RNA motif–ligand interactions that allows simultaneous screening of both RNA and chemical space. We used this platform to identify the RNA internal loops that bind 6′-*N*-5-hexynoate kanamycin A (**1**). Selected internal loops that bind **1** were studied in detail and commonly display an adenine across from a cytosine independent of the size of the loop. Additional preferences are also observed. For 3 × 3 nucleotide loops, there is a preference for purines, and for 2 × 2 nucleotide loops there is a preference for pyrimidines neighbored by an adenine across from a cytosine. This technique has several advantageous features for selecting RNA motif–ligand interactions: (1) higher affinity RNA motif–ligand interactions are identified by harvesting bound RNAs from lower ligand loadings; (2) bound RNAs are harvested from the array via gel extraction, mitigating kinetic biases in selections; and (3) multiple selections are completed on a single array surface. To further demonstrate that multiple selections can be completed in parallel on the same array surface, we selected the RNA internal loops from a 4096-member RNA internal loop library that bound a four-member aminoglycoside library. These experiments probed 16,384 (4 aminoglycoside × 4096-member RNA library) interactions in a single experiment. These studies allow for parallel screening of both chemical and RNA space to improve our understanding of RNA–ligand interactions. This information may facilitate the rational and modular design of small molecules targeting RNA.

RNA forms complex tertiary structures that impart diverse functions (*1, 2*). For example, RNA catalyzes reactions (*3*), regulates gene expression (*4, 5*), encodes protein, and plays other essential roles in biology. Therefore, RNA is an interesting and important target for developing drugs or probes of function (*6, 7*). It is a vastly underutilized target, however, mainly because of the limited information available on RNA–ligand interactions that could facilitate rational design.

One advantage of using RNA as a drug target is that secondary structure information, which includes the motifs that comprise an RNA, can be easily obtained from sequence by free energy minimization (*8, 9*) or phylogenic comparison (*10*). RNA tertiary structures are composites of the secondary structural motifs and the long-range contacts that form between them. Furthermore, RNA motifs can have similar properties both as isolated systems and as parts of larger RNAs. For example, aminoglycoside antibiotics affect the structure of the bacterial rRNA A-site similarly when they bind the entire ribosome or an oligonucleotide mimic of the bacterial rRNA A-site (*11–16*). Studies on the binding of aminoglycosides and streptamine dimers to RNA hairpins (*17–20*) have facilitated the development of compounds to combat multidrug resistance by causing plasmid incompatibility (*19, 20*). These results show that the identification of RNA motifs that bind small molecules can be useful for targeting the larger RNAs that contain them.

In order to understand how to target RNA with small molecules, a large data set of RNA-ligand interactions is required. This is due to the diverse structures that RNA adopts, internal and hairpin loops for example. Current methods to study and identify RNA–ligand interactions include systematic evolution of ligands by exponential enrichment (SELEX) (*21, 22*), structure–activity relation-

*Corresponding author, mddisney@buffalo.edu.

Received for review August 13, 2007 and accepted October 15, 2007.

Published online November 2, 2007

10.1021/cb700174r CCC: $37.00

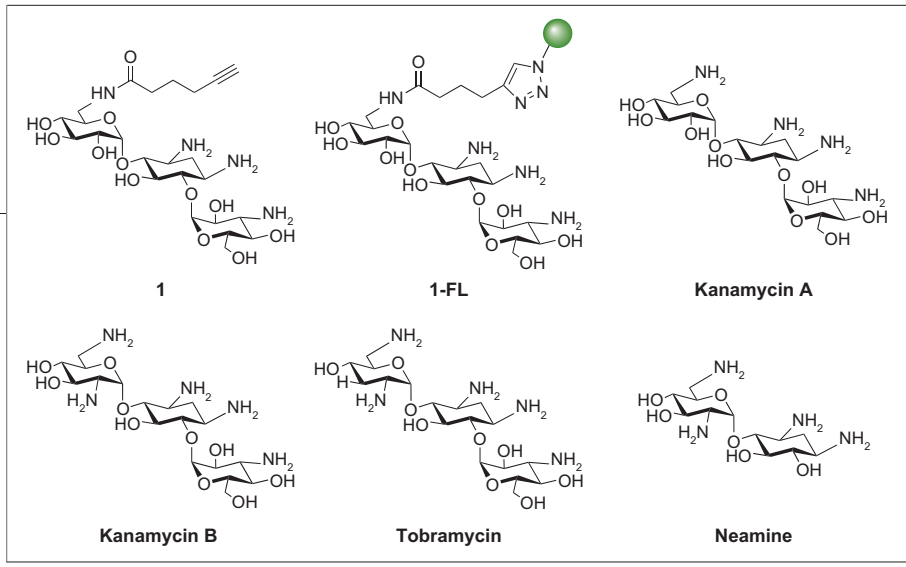

Figure 1. Structures of the aminoglycosides and derivatives thereof used in these studies. Compound 1 **is 6′-*N*-5-hexynoate kanamycin A and was used in selection experiments.** 1-FL **is** 1 **conjugated to fluorescein via a Huisgen dipolar cycloaddition reaction; the dye is indicated with the green ball.** 1-FL **was used in fluorescence assays to determine dissociation constants. Kanamycin A, kanamycin B, tobramycin, and neamine were used in competitive binding experiments to determine aminoglycoside preferences for selected internal loops.**

ships (SAR) by mass spectrometry (MS) (*23–26*) and NMR (*27*), and chemical microarrays (*28–30*). These methods probe RNA space (SELEX) or chemical space (SAR by MS and NMR and chemical microarrays) separately. A more desirable method would screen chemical and RNA space simultaneously. One way to do this would be to merge nucleic acid selections with chemical or carbohydrate microarray-based ligand screening.

Herein, we describe a microarray platform to complete nucleic acid selections that combines the advantages of selection methods and small molecule microarrays. Our basic approach is to immobilize ligands onto an agarose microarray surface and screen the ligands for binding to an RNA motif library. The RNAs that bind members of the ligand library are harvested directly from the array surface by gel excision, cloned, and identified via sequencing. This approach was applied toward identifying the RNA internal loops that bound 6′-*N*-5-hexynoate kanamycin A (**1**, Figure 1). Results show that **1** binds to internal loops that can form potential CA pairs. All selected RNA internal loops bind **1** with K_d values $\leq$22 nM.

RESULTS AND DISCUSSION

The Microarray Platform and the RNA Library. Successful merging of nucleic acid selections and small molecule microarrays required a unique microarray surface that is robust enough for ligand screening and allows bound RNAs to be harvested directly from the array surface. We found that the optimal surface for this application is an agarose-coated microarray (*31–33*). Agarose provides a three-dimensional surface for high ligand loading and a versatile surface to accommodate a variety of immobilization chemistries, and bound RNAs can be harvested from the array surface by simple excision of the agarose from ligand-functionalized positions (Figure 2).

The RNA library (**2**) that was screened for binding **1** has six randomized positions displayed in a 3 × 3 nucleotide internal loop pattern (Figure 3) (*34*). By selecting RNAs from this library, we focus selections only on small RNA motifs that are likely to be found as constituents of larger RNAs. This is in contrast to SELEX, which uses libraries with ~15 randomized nucleotides. These 15-mers are very difficult to find in biological RNAs; however, in rare occasions SELEX has proven successful in RNA-targeting endeavors (*35, 36*). Library **2** has 4096 members that can form a variety of internal loops and also base paired regions. Specifically, **2** contains 1600 different 3 × 3 internal loops, 1200 different 2 × 2 loops, 1080 different 1 × 1 loops, and 216 different base paired regions. These values were calculated by assuming that a GU pair is a standard RNA pair

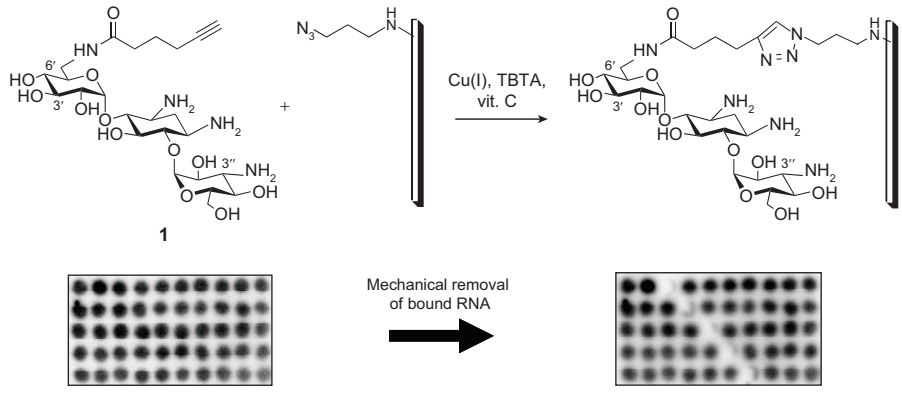

Figure 2. (Top) Schematic of the immobilization of 1 **onto azide-functionalized agarose slides via a Huisgen dipolar cycloaddition reaction. (Bottom) Representative autoradiograms of (left) an array hybridized with radioactively labeled** 2 **and (right) an array after excision of bound RNAs. Bound RNAs can be amplified by RT-PCR, cloned, and sequenced.**

and that two 1 × 1 internal loops cannot be separated by a base pair; these structures are counted as 3 × 3 loops.

Development of the Microarray Selection Method. An array containing 50 ligand-functionalized spots was constructed by immobilizing **1** onto azide-functionalized surfaces via a Huisgen dipolar cycloaddition reaction (*37*, *38*). The array was then probed for binding to 5′ end ^{32}P-labeled **2**. All positions where **1** was immobilized bound members of **2** with similar intensities (Figure 2). A diagonal of spots was excised from the array to assess if bound RNAs can be harvested precisely without affecting adjacent spots. Images of the array taken before and after excision show that RNA was harvested only from the desired positions and that signals in the surrounding spots were unaffected (Figure 2); thus there is no cross-contamination between spots. Harvested RNA is suitable for amplification by reverse transcriptase polymerase chain reaction (RT-PCR), cloning, and sequencing to identify the selected library members (Figure 4).

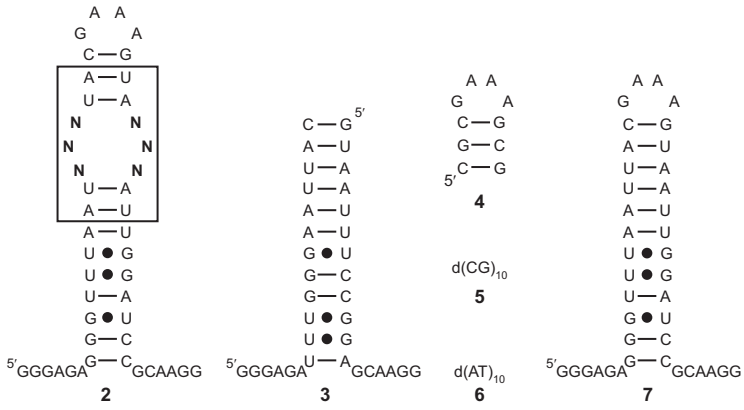

Figure 3. Oligonucleotides used to identify the RNA internal loops that bind 1. Oligonucleotide 2 is the internal loop library with six randomized positions (N). The library has 4096 unique members. Oligonucleotides 3–6 were used at 1000 times the concentration of 2 in selection experiments to ensure that interactions occurred to loop nucleotides and not to the cassette. 3 is a mimic of the stem in 2. The sequence was altered such that it does not compete for RT-PCR primers. 4 is a mimic of the GAAA hairpin in 2. 5 and 6 are DNA oligonucleotides that ensure interactions are RNA specific. 7 is the cassette in which the internal loop library is embedded.

Next, we immobilized serially diluted concentrations of **1** onto azide-agarose and incubated the slide with 5′ end ^{32}P-labeled **2** and unlabeled chase oligonucleotides (Figure 3). Chase oligonucleotides included a mimic of the stem (**3**) and hairpin (**4**) in **2** and DNAs that formed d(GC) (**5**) and d(AT) (**6**) Watson–Crick pairs. This combination was used to ensure that only internal loop-small molecule interactions were probed in the selection and that interactions were RNA-specific. For the experiments in Figure 4, chase oligonucleotides were added in 1000-fold excess over **2** and in excess over the amount of ligand delivered to the array surface. Under these conditions, concentration-dependent binding is observed to **2** with signals that are well above background (Figure 4, panels a and b). Six samples were collected from the surface where different amounts of **1** were immobilized (Figure 4, panel a) and amplified by RT-PCR (Figure 4, panel c). RT-PCR product was only observed when samples were taken from positions functionalized with **1** and when RT was added to the RT-PCR reactions. No RT-PCR product was observed when samples were taken from a position where **1** was not delivered or when RT was not added to the RT-PCR reaction, provided ≤30 cycles of PCR were used.

One advantage of screening different concentrations or loadings of ligands is higher affinity RNA motif–ligand interactions should be identified at lower ligand loadings. To determine if this is indeed the case, we studied the binding of the pools of RNAs harvested from 1+ (higher ligand loading) and 2+ (lower ligand loading) by using a fluorescence-based assay. Compound **1** was fluorescently labeled (**1-FL**, Figure 1) by reacting Boc-protected **1** with propargylamine using the Huisgen dipolar cycloaddition reaction used to anchor **1** onto the array surface. The product of this reaction was reacted with fluorescein isothiocyanate to yield **1-FL** (details in Supporting Information). Dissociation constants for the binding of **1-FL** to the library of RNAs was determined because the fluorescence emission of **1-FL** decreased as a function of RNA concentration. The resulting curves were used to determine dissociation constants. Results show that K_d values for 1+ and 2+ are 65 nM and 11 nM, respectively (Figure 4). Evidently,

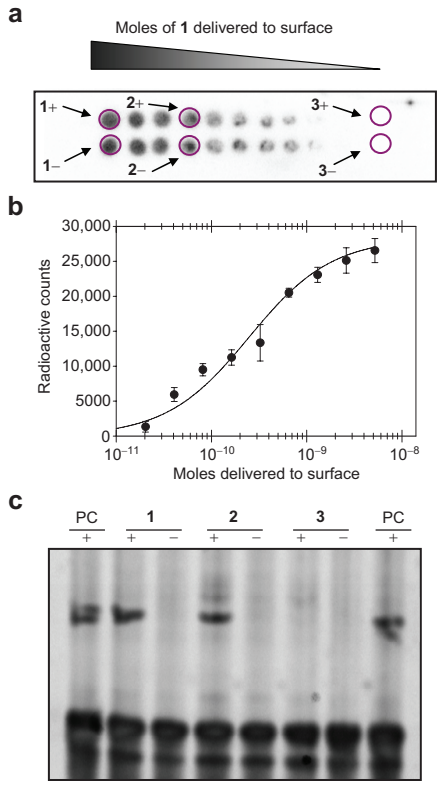

Figure 4. a) Image of an array after hybridization with 10 nM of 5′ end ^{32}P-labeled 2 and 10,000 nM each of 3–6. b) the dose–response curve for binding to 1 in the presence of 3–6 on the array. The extracted positions are circled. c) Results from RT-PCR amplification of RNA harvested from the array. "+" indicates RT was added to the RT-PCR reaction. "–" indicates RT was not added to the RT-PCR reaction. PC is a positive control for RT-PCR. The top bands on the gel are RT-PCR products while the bottom bands are primers. The affinities of 1 for RNAs from position 1+ and 2+ are 65 nM and 11 nM, respectively.

RNAs harvested at a lower ligand loading have higher affinities for **1**.

Since RNAs harvested from the surface can be RT-PCR amplified and subsequently used as templates for runoff transcription, multiple rounds of selection can be completed if desired. The ability to complete selections at different ligand loadings on the same surface demonstrates that this platform can be used to complete multiple selections in parallel on a single array.

To further illustrate that multiple selections can be completed on a single agarose array platform, we immobilized a four-member azido-aminoglycoside library (Figure 5, **8**–**11**) onto alkyne-functionalized agarose (*37, 39*) and selected members of **2** that they bound. Each aminoglycoside was immobilized at five different loadings and probed for binding **2** in the presence of **3**–**6.** Members of **2** bound to these structures with signals that depend on both the aminoglycoside loading and identity. Bound RNAs at the indicated positions in Figure 5 were harvested and were cleanly RT-PCR amplified over positions excised from where aminoglycoside was not delivered to the array surface (background) (N.C., Figure 5). When only the number of aminoglycosides are considered for binding **2**, 4×4096, or 16,382, interactions were probed in duplicate; however if the number of aminoglycosides (four) and their loadings (five each) are considered, $4 \times 5 \times 4096$, or 81,920, interactions were probed in duplicate.

Analysis of the Sequences of the Selected Structures That Bind 1. Selected higher affinity RNAs from 2+ (Figure 4) were cloned and sequenced, and their secondary structures predicted by free energy minimization using the RNAstructure program (Figure 6) (*8*). Interestingly, many of the selected loops share sequence similarities. There is a clear preference for loops with adenine across from cytosine. (We state adenine across from a cytosine rather than A-C pair to denote that we do not know if these bases are indeed paired.) Of the 16 loops identified from the selection, 10 (62.5%) contain at least one adenine across from a cytosine, in contrast to only 33% of all library members (two-tailed p-value $= 0.0124$) (details in Supporting Information). For each internal loop class, the selection of at least one adenine across from an cytosine is above the rate if the selection were random: 60% of 1×1 nucleotide internal loops, 66% of 2×2 nucleotide internal loops, and 60% of 3×3 nucleotide internal loops. Of the 1080 1×1 nucleotide internal loops in **2**, 20% have an adenosine across from a cytosine; 36% of 2×2 nucleotide internal loops contain at least one adenosine across from a cytosine; 44% of 3×3 nucleotide internal loops contain at least one adenosine across from a cytosine. For the entire library, **2**, 33% of the loops contain at least one adenosine across from a cytosine. (See Supporting Information for calculations.)

Other sequence preferences are also observed. For the 2×2 nucleotide loops, the predicted lowest free energy structures show preferences for pyrimidines neighbored by adenine across from cytosine (two-tailed p-value $= 0.0093$). The preference for pyrimidines in

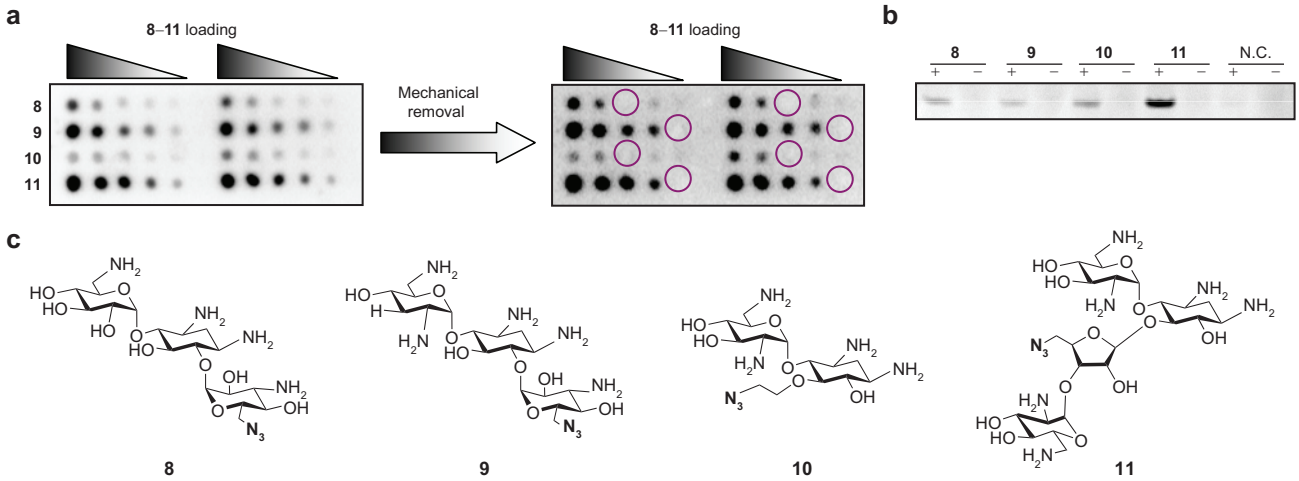

Figure 5. Two-dimensional combinatorial screen of an array-immobilized aminoglycoside library for binding to members of 2. a) Image of an array after hybridization with ^{32}P-labeled 2 and unlabeled 3–6. Bound RNAs were mechanically removed from the agarose surface at the positions indicated with circles. b) Results from RT-PCR amplification of the samples removed in panel a. N.C. is a negative control RT-PCR reaction from background or nonaminoglycoside functionalized agarose. c) Structures of the four azido-aminoglycosides that were anchored onto alkyne-functionalized agarose and probed for binding to the RNA library. By screening four compounds at five loadings for binding 1, we probed 4 × 4096, or 16,382, interactions in duplicate when we only consider the different compounds or 4 × 5 × 4096, or 81,920, interactions in duplicate when we consider both the compounds and their loadings. These experiments were completed in 20 mM HEPES (pH 7.5), 150 mM NaCl, 5 mM KCl, and 1 mM $MgCl_2$ (HBII).

2 × 2 nucleotide internal loops was also observed in our resin-based selection (*40*). Interestingly, many of the 1 × 1 and 2 × 2 nucleotide internal loops are closed by G◦U base pairs. The predicted lowest free energy structures of the 3 × 3 nucleotide loops also show a preference for purines (two-tailed *p*-value = 0.0309). In fact, for the two 2 × 2 and two 3 × 3 nucleotide internal loops that do not contain an adenine across from a cytosine, three of them contain either a guanine across from a guanine or a cytosine across from a cytosine, which are both observed in the 1 × 1 loops. This may suggest that the motifs displayed in the 1 × 1 nucleotide loops are also displayed in the 3 × 3 nucleotide loops. The one 2 × 2 nucleotide loop that does fit either criterion (**IL 8**) has tandem guanines across from adenines, which are displayed in many of the selected 3 × 3 nucleotide loops (**IL 12**, **IL 13**, and **IL 15**). The exact pairings that give rise to these structural features will have to be determined through structural investigations, but it will be interesting to see if these sequences display a similar RNA structural scaffold to bind **1**.

Measuring the Affinities of Selected Structures to 1-FL. The affinity of each loop was determined using the fluorescence assay described above. Each selected internal loop binds to **1** with a similar affinity, all with K_d values ≤22 nM (Figure 6). The range of dissociation constants (5–22 nM) corresponds well to the dissociation constant determined for the pool of RNAs harvested from position 2+ (11 nM). In contrast, **1-FL** binds more weakly to the chase oligonucleotides and the library. The fluorescence intensity of **1-FL** did not change in the presence of **3**, **4**, and **5**+**6** at concentrations up to 5 μM (Figure 2). The affinity for **2** (the entire library) was 280 nM while the affinity for the empty cassette, **7**, was 1.3 μM. Interactions between **1-FL** and **7** likely occur between the deoxystreptamine ring and G◦U pairs in the stem, which have been reported as aminoglycoside interacting motifs in other RNAs that bind aminoglycosides (*41*). $tRNA^{phe}$ has also been shown to bind aminoglycosides (*42*) and binds **1-FL** with a K_d of 700 nM.

The dissociation constants for the two highest affinity loops from our resin-based selection were also determined using the fluorescence-based assay. Both loops, $^{5'UUU3'}_{3'UCA5'}$ and $^{5'ACU3'}_{3'UUU5'}$, bind as tightly to **1-FL** as the highest affinity 2 × 2 loop from the microarray selection with dissociation constants of 5 ± 0.4 and 4 ± 0.9 nM, respectively.

The affinities of the 1 × 1 nucleotide loops for **1-FL** have a range of 5−12 nM (Figure 6), and GG, AC, and CC loops are represented. It should be noted that previ-

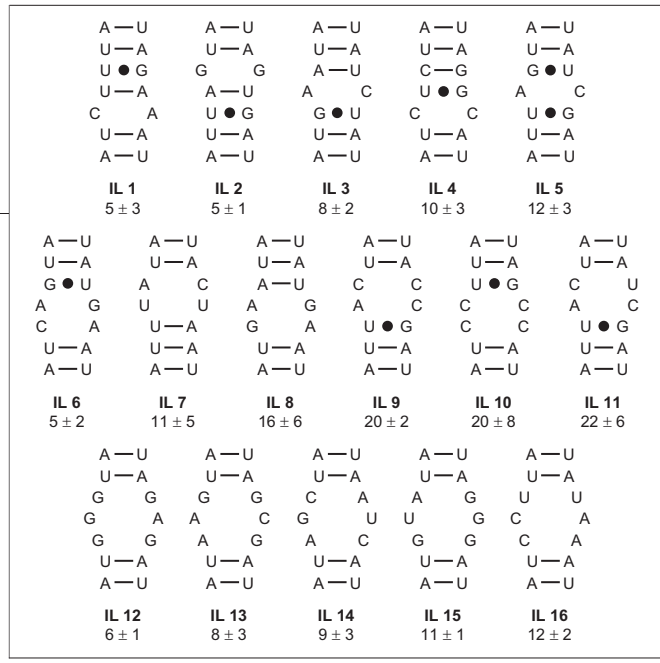

Figure 6. Secondary structures of the internal loops selected to bind 1. The secondary structures were the lowest free energy structures predicted by the program RNAstructure (*8, 9*). The nucleotides shown are derived from the boxed region in 1 (Figure 2). The dissociation constants (nM) were determined from fluorescence assays. The K_d values for oligonucleotides 2, 3, 4, 5 + 6, and 7 are 280 nM, >5 μM, >5 μM, >5 μM, and 1.3 μM, respectively. The K_d for tRNA^{phe} is 0.7 μM. For each selected internal loop, the binding curves indicate a stoichiometry of 1:1 (details in Supporting Information).

ous experiments have also found that several aminoglycosides bind a 1 × 1 CC internal loop that is derived from the untranslated region in thymidylate synthase mRNA (*43, 44*). In these previous reports, the dissociation constants for kanamycin B and tobramycin were 1.1 and 0.87 μM, respectively, in a buffer containing 1 mM $MgCl_2$ and $CaCl_2$, 150 mM NaCl, 5 mM KCl, and 20 mM HEPES (pH 7.5) (*44*). We studied the binding of **1-FL** to **IL 4** in the same buffer and observed a similar affinity (K_d of 0.21 ± 0.04 μM) despite differences in closing base pairs and aminoglycoside structure (details in Supporting Information). The difference in binding affinity between the two buffers is due to the presence of divalent metal ions and increased pH, which are well-known to decrease the affinity of aminoglycosides to RNA (*17*).

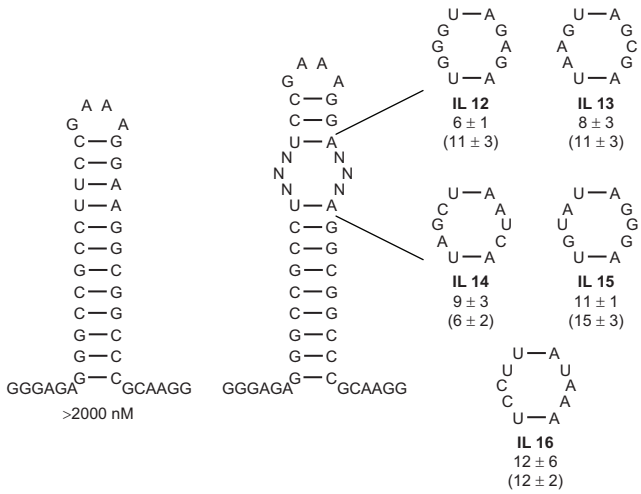

Figure 7. Secondary structure of the cassette with all GU and most AU pairs mutated to GC used to determine if loop non-nearest neighbors contribute to binding affinity. The loop-closing base pairs were not mutated since they have been shown to affect loop structure. The dissociation constants for the loops in the mutated cassette are directly below the loop number and are reported in nM. The dissociation constants when the loops are displayed in 2 are in parentheses.

Because deoxystreptamine binds G◦U pairs, the stem in **2** was mutated to assess if loop non-nearest neighbors contribute to binding affinity (Figure 7). All G◦U pairs and most AU pairs were mutated to GC. The loop-closing base pairs (both AU pairs) were not mutated because previous reports have shown that closing base pairs can affect internal loop structure (*45, 46*). Results from fluorescence experiments show that similar K_d values are observed when the loops are displayed in either cassette (Figure 7). Evidently, cassette nucleotides are not important for recognition of the selected loops by **1-FL**.

To determine if selected loops have aminoglycoside preferences, the binding of five aminoglycosides (**1**, kanamycin A, kanamycin B, tobramycin, and neamine, Figure 1) to the pool of RNAs from spot 2+ (Figure 4) was probed using a competitive binding assay (*43*, details in Supporting Information). The K_d values determined for **1**, kanamycin A, and kanamycin B were 12 nM, 9 nM, and 12 nM, respectively. The pool bound approximately 9-fold more weakly to tobramycin (K_d = 85 nM), consistent with the 3′ hydroxyl group in ring I contributing to binding to the library of structures. Binding to neamine was even weaker as there was no change in fluorescence up to 500 nM neamine. We also tested a single RNA sequence identified to bind **1**, **IL 14**, in the same manner. These experiments mirror the results of the pool of RNAs isolated from 2+, showing that **1**, kanamycin A, and kanamycin B bind to **IL 14** with K_d values of 7, 5, and 5 nM, respectively. Binding to neamine and tobramycin was also much weaker (details in Supporting Information). Both sets of experiments suggest that the recognition of **1** and related aminoglycosides (kanamycins A and B) is not due to simple charge–charge interactions; rather, there are specific interactions between the functional groups displayed by the

aminoglycosides and the RNA. The weaker affinities for tobramycin and neamine suggest that both the 3′ hydroxyl groups in ring I and ring III are important for binding. Interestingly, in both cases, **1** and **1-FL** bind with the same affinity showing that the fluorescence tag, the triazole, and the 6′ NH_2 groups do not contribute significantly to binding. It is not surprising that the 6′ NH_2 is not important for binding since structures were selected that bind a 6′ acylated derivative of kanamycin A. It should be noted, however, that the 6′ NH_2 forms important stabilizing contacts for aminoglycoside recognition of the bacterial rRNA A-site. When the 6′ NH_2 is acetylated by AAC(6′) resistance enzymes, binding to an oligonucleotide mimic of the bacterial rRNA A-site is reduced 1000-fold (*47*). Therefore, there are differences in the molecular recognition of **1** to **IL 14** and kanamycin A to the bacterial rRNA A-site.

Advantages of the Microarray Selection Platform. The microarray selection platform has several advantages over other selection methods. One is the manner in which selected RNAs are harvested. In typical resin-based selections, selected RNAs are eluted with a high concentration of immobilized ligand which can introduce potential kinetic biases. Since the highest affinity RNAs are the most difficult to compete off, standard selection experiments can inadvertently miss the best binders. Capillary electrophoresis (CE) SELEX has been developed to mitigate this problem (*48*). The microarray method described herein harvests bound RNAs by simple excision of the agarose and gel extraction (Figure 2), thus avoiding potential kinetic biases. RNAs can be harvested precisely from the microarray surface; adjacent spots are unaffected and the RNAs are free from cross-contamination (Figure 2). Therefore, the RNA is suitable for downstream applications such as RT-PCR amplification and cloning, transcription of RT-PCR products, multiple rounds of selection, and determination of dissociation constants. Another important advantage of completing selections on a microarray platform is the ability to determine dose response on a single array (Figure 4). Standard selection methods only screen a library of nucleic acids against one compound at a single loading. Therefore, a separate experiment for each ligand loading is required to construct a dose response. In this study, higher affinity interactions were identified at a lower ligand loading (Figure 4, panel a). This result and the ones shown in Figure 5 demonstrate that multiple selections can be completed on a single array surface. The number of parallel screens is limited by the number of compounds that can be placed onto an array surface from which bound RNAs can be subsequently isolated. With manual methods, the minimum number of compounds that can be screened is on a 1 × 3 in. slide with ~3 mm spot diameters is ~50. It is likely that robotic arraying of compounds and using automated spot pickers to harvest bound RNAs could increase this number to at least hundreds of compounds. Finally, the microarray method requires a reduced amount of ligand compared to resin-based selections. Selected RNAs were amplified from positions where as little as 250 pmol of ligand were delivered to the array surface (Figure 4, spot 2).

Summary and Outlook. Our long-range goal is to develop a database of RNA−ligand partners to facilitate the rational design of small molecules that target RNA (*40*). Clearly, new methods need to be developed because of the diverse number of RNA secondary structures and ligands that must be screened to construct such a database. Therefore, we developed a small molecule carbohydrate microarray platform to identify RNA−ligand interactions in which multiple selections and dose response can be completed in a single experiment. Traditional ligand discovery efforts screen a validated RNA drug target against a ligand library. This type of screen, however, gives little insight into potential off-target effects. Our microarray platform screens a library of RNAs to determine the RNA motif(s) preferred by a ligand. These preferences can then be used in RNA targeting applications while identifying potential bystander RNAs.

Once a wide variety of RNA motif−ligand interactions have been identified, methods for modular assembly of ligands can be developed, such as those applied by the Dervan group for polyamide recognition of Watson–Crick paired DNA (*49*). Microarray-based screening is well suited for identifying ligands that will be used for modular assembly because chemistries used to anchor compounds onto surfaces can be used to link ligand modules together. Results from these and other studies using this platform will be disclosed in due course.

METHODS

General Methods. Chemicals were purchased from Sigma Aldrich, except radioactivity which was purchased from Perkin-Elmer. Chase RNA oligonucleotides were purchased from Dharmacon and were deprotected using the manufacturer's standard protocol. The chase DNA oligonucleotides (**5** and **6**, Figure 3) and all DNA templates were purchased from Integrated DNA Technologies (IDT). The RNA 3 × 3 nucleotide internal loop library was transcribed from a DNA template using T7 RNA polymerase (*50*) from a Stratagene RiboMaxx transcription kit. Oligonucleotides were radioactively labeled on their 5′ ends and purified as described (*51*). All solutions were made with DEPC-treated water.

Microarray Construction, Hybridization, and Harvesting Bound RNAs from the Agarose-Functionalized Array. The 6′-*N*-5-hexynoate kanamycin A ligand (**1**) was spotted in 10 mM sodium phosphate, pH 7.5, 1 mM TCEP, 1 mM $CuSO_4$, 100 μM TBTA ligand (*37*), and 10% glycerol onto azide-displaying agarose slides (*31*) constructed as described (*40*). Azidoaminoglycosides (**8**–**11**) were immobilized onto alkyne-functionalized agarose surfaces as described (*52*). The alkyne-functionalized arrays were constructed as described (*40*) except that propargylamine was used instead of 3-azidopropylamine. A grid affixed to the back of the microarray was used as a guide for spatial arraying. After immobilization, the grid was removed, and the slides were incubated overnight in a humidity chamber. The following morning, they were washed by submersion in 30 mL of hybridization buffer (HBI) (8 mM Na_2HPO_4, pH 7.0, 185mM NaCl, and 1 mM EDTA) and then rinsed with water.

Microarrays were hybridized with a solution containing 5′ end ^{32}P-labeled RNA 3 × 3 nucleotide library (**2**) and chase oligonucleotides (Figure 3). Chase oligonucleotides were used to ensure that RNA internal loop−ligand interactions were probed. Each oligonucleotide (2 pmol of 5′ end ^{32}P-labeled RNA 3 × 3 internal loop library (**2**), 2 nmol of each chase oligonucleotide for experiments with **1** and 12 pmol of internally labeled **2** (α-^{32}P-ATP, transcription with Stratagene RNAMaxx kit using half of the suggested cold ATP and 4 μL of ^{32}P-ATP or 40 μCi) and 20 nmol of each chase oligonucleotide for experiments with **8**–**11**) was annealed separately in HBI for experiments with **1** and HBII (20 mM HEPES (pH 7.5), 150 mM NaCl, 5 mM KCl, and 1 mM $MgCl_2$) for experiements with **8**–**11** by heating at 95 °C for 1 min and cooling to RT on the benchtop. After cooling to RT, the solutions containing each oligonucleotide were mixed together and 40 μg/mL BSA was added in a total volume of 400 μL.

Prior to hybridization, arrays were pre-equilibrated with 400 μL of hybridization buffer containing 40 μg/mL of BSA for 5 min. The buffer was distributed evenly across the array surface using a custom-cut piece of Parafilm that was placed over the applied solution. The Parafilm and buffer were then removed. The solution containing **2** and chase oligonucleotides was applied to the array surface and distributed evenly as described above. Slides were hybridized for approximately 30 min at RT. After incubation, the Parafilm was removed from the slide, and the slide was submerged in 30 mL of hybridization buffer for 3 min with gentle agitation. The buffer was replaced, and the step was repeated. The residual buffer was removed from the array surface by applying a gentle stream of air, and the chip was allowed to remain at RT for 30 min to dry completely. The array was exposed to a phosphorimager plate that was scanned on a BioRad FX phosphorimager (Figure 2).

An autoradiogram of the array and a grid used to spot **1** were placed under the microarray as a template to excise the agarose at positions that captured RNA. A 200 nL aliquot of hybridization buffer was added to each position. After 30 s, excess buffer not absorbed by the surface was removed. The gel slice at that position was then excised using a toothpick, and the gel slice was placed into thin-walled PCR tubes with 18 μL of H_2O, 2 μL of 10x DNase I buffer, and 2 units of RNase-free DNase I (Promega). The tubes were vortexed and spun at 8000*g* for 4 min to force the agarose to the bottom of the tube. The solution was incubated at 37 °C for 2 h, and the reaction was quenched by addition of 2 μL of 10x DNase stop solution. The sample was then incubated at 65 °C for 10 min to inactivate completely the DNase. Aliquots of this sample were RT-PCR amplified as described (Supporting Information). We found that spot 2 (250 pmol of **1** delivered to the surface) was the lowest amount of ligand from which captured RNA can be amplified over the background (spot 3+) (Figure 4). RT-PCR product was observed after 25 cycles of PCR following the RT step. Attempts were made to amplify positions where lower amounts of **1** were delivered, but they required >35 cycles for amplification. Under these conditions, RT-PCR product was observed from positions where **1** was not delivered. We therefore only processed the 2+ position.

RNA Internal Loop−Ligand Interaction Affinity Measurements.

Direct Binding Assay Measurements. A fluorescence-based assay was used to determine binding affinities by monitoring the change in fluorescence intensity of **1-FL** (Figure 1) as a function of RNA concentration (up to 300 nM for selected loops; there is a nonspecific binding mode at concentrations >300 nM). RNA was annealed in 1X HB + 40 μg/mL BSA at 60 °C for 5 min and allowed to slow cool on the benchtop. Then, **1-FL** in 1X HB + 40 μg/mL BSA was added to the solution of RNA to a final concentration of 10 nM, and the RNA serially diluted into 1X HB + 40 μg/mL BSA + 10 nM **1-FL**. Samples were then placed into a well of a black 96-well plate and allowed to equilibrate for at least 30 min before reading fluorescence intensity on a Bio-Tek Synergy HT fluorescence plate reader (excitation, 485 nm; emission, 528; sensitivity, 70). Several different times were sampled to ensure that the fluorescence intensity was taken after these interactions reached equilibrium. A decrease in fluorescence intensity was observed as a function of RNA concentration. The binding measurements for each oligonucleotide were completed in at least triplicate. Dissociation constants were determined by curve fitting, and reported values are the mean of at least three experiments. The data were fit to:

$$I = I_0 + 0.5\Delta\epsilon(([\mathbf{1\text{-}FL}]_0 + [\mathrm{RNA}]_0 + K_t) - (([\mathbf{1\text{-}FL}]_0 + [\mathrm{RNA}] + K_t)^2 - 4[\mathbf{1\text{-}FL}]_0[\mathrm{RNA}]_0)^{0.5})$$

where I is the observed fluorescence intensity, I_0 is the fluorescence intensity in the absence of RNA, $\Delta\epsilon$ is the difference between the fluorescence intensity in the absence of RNA and in the presence of infinite RNA concentration, $[1\text{-FL}]_0$ is the concentration of **1-FL**, $[\mathrm{RNA}]_0$ is the concentration of the selected internal loop or control RNA, and K_t is the dissociation constant. Plots and curve fitting for a representative internal loop and chase oligonucleotides are available (Supporting Information). We also plotted the change in fluorescence as a function of RNA equivalents for all selected internal loops. Saturation is observed between 0.8 and 1.3 equiv, suggesting a 1:1 stoichiometry (details in Supporting Information). Control experiments were completed to ensure that fluorescein (the fluorescent tag) was not contributing to binding by incubating serial dilutions of **IL 4** up to 3 μM with 10 nM FITC-triazole and 10 nM fluorescein (details in Supporting Information).

Competition Binding Experiments. A solution containing 75 nM **IL 14** was refolded in 1X hybridization buffer + 40 μg/mL BSA at 60 °C for 5 min. After slow cooling on the benchtop, **1-FL** was added to a final concentration of 10 nM. The competing, unlabeled aminoglycoside was then added, and the resulting solution was serially diluted into 1X hybridization buffer + 40 μg/mL BSA + 10 nM **1-FL** containing 75 nM **IL 14**. The solutions were equilibrated for 30 min

at RT, and the fluorescence intensities were measured on a Bio-Tek HT fluorescence plate reader. Data were fit to:

$$\Theta = \frac{1}{2[\mathbf{1\text{-}FL}]}[K_t + \frac{K_t}{K_d}[C_t] + [RNA] + [\mathbf{1\text{-}FL}] - \sqrt{\left(K_t + \frac{K_t}{K_d} + [C_t] + [RNA] + [\mathbf{1\text{-}FL}]\right)^2 - 4[\mathbf{1\text{-}FL}][RNA]} + A$$

where Θ is the fraction of **1-FL** bound, K_t is the dissociation constant determined for **IL 14** from direct binding assays, K_d is the dissociation constant of the competing, unlabeled aminoglycoside, $[C_t]$ is the concentration of competing aminoglycoside, and [RNA] is the concentration of **IL 14**. Plots and curve fitting of competition experiments are available (Supporting Information).

Acknowledgment: J.L.C.-D. and M.D.D. dedicate this paper to our friend and mentor Doug Turner. We thank Joaquin Carbonara, Mitra Feizabadi, and Richard Cheng for helpful discussions. We also thank the Camille and Henry Dreyfus Foundation (New Faculty Award to M.D.D.), NYSTAR (JD Watson Young Investigator Award to M.D.D.), the Kapoor Funds, The New York State Center of Excellence in Bioinformatics and Life Sciences, and The University at Buffalo for providing funding for this work.

Supporting Information Available: This material is free of charge *via* the Internet.

REFERENCES

1. Doudna, J. A. (2000) Structural genomics of RNA, *Nat. Struct. Biol. 7 Suppl.*, 954–956.
2. Batey, R. T., Rambo, R. P., and Doudna, J. A. (1999) Tertiary motifs in RNA structure and folding, *Angew. Chem., Int. Ed. Engl. 38*, 2326–2343.
3. Zaug, A. J., and Cech, T. R. (1986) The intervening sequence RNA of tetrahymena is an enzyme, *Science 231*, 470–475.
4. Lagos-Quintana, M., Rauhut, R., Lendeckel, W., and Tuschl, T. (2001) Identification of novel genes coding for small expressed RNAs, *Science 294*, 853–858.
5. Winkler, W., Nahvi, A., and Breaker, R. R. (2002) Thiamine derivatives bind messenger RNAs directly to regulate bacterial gene expression, *Nature 419*, 952–956.
6. Gallego, J., and Varani, G. (2001) Targeting RNA with small-molecule drugs: therapeutic promise and chemical challenges, *Acc. Chem. Res. 34*, 836–843.
7. Hamy, F., Felder, E. R., Heizmann, G., Lazdins, J., Aboul-ela, F., Varani, G., Karn, J., and Klimkait, T. (1997) An inhibitor of the Tat/TAR RNA interaction that effectively suppresses HIV-1 replication, *Proc. Natl. Acad. Sci. U.S.A. 94*, 3548–3553.
8. Mathews, D. H., Disney, M. D., Childs, J. L., Schroeder, S. J., Zuker, M., and Turner, D. H. (2004) Incorporating chemical modification constraints into a dynamic programming algorithm for prediction of RNA secondary structure, *Proc. Natl. Acad. Sci. U.S.A. 101*, 7287–7292.
9. Mathews, D. H., Sabina, J., Zuker, M., and Turner, D. H. (1999) Expanded sequence dependence of thermodynamic parameters improves prediction of RNA secondary structure, *J. Mol. Biol. 288*, 911–940.
10. Woese, C. R., Magrum, L. J., Gupta, R., Siegel, R. B., Stahl, D. A., Kop, J., Crawford, N., Brosius, J., Gutell, R., Hogan, J. J., and Noller, H. F. (1980) Secondary structure model for bacterial 16S ribosomal RNA: phylogenetic, enzymatic and chemical evidence, *Nucleic Acids Res. 8*, 2275–2293.
11. Fourmy, D., Recht, M. I., Blanchard, S. C., and Puglisi, J. D. (1996) Structure of the A-site of Escherichia coli 16S ribosomal RNA complexed with an aminoglycoside antibiotic, *Science 274*, 1367–1371.
12. Lynch, S. R., Gonzalez, R. L., and Puglisi, J. D. (2003) Comparison of X-ray crystal structure of the 30S subunit-antibiotic complex with NMR structure of decoding site oligonucleotide-paromomycin complex, *Structure (Cambridge, MA, US) 11*, 43–53.
13. Carter, A. P., Clemons, W. M., Brodersen, D. E., Morgan-Warren, R. J., Wimberly, B. T., and Ramakrishnan, V. (2000) Functional insights from the structure of the 30S ribosomal subunit and its interactions with antibiotics, *Nature 407*, 340–348.
14. Kaul, M., Barbieri, C. M., and Pilch, D. S. (2006) Aminoglycoside-induced reduction in nucleotide mobility at the ribosomal RNA A-site as a potentially key determinant of antibacterial activity, *J. Am. Chem. Soc. 128*, 1261–1271.
15. Kaul, M., Barbieri, C. M., and Pilch, D. S. (2004) Fluorescence-based approach for detecting and characterizing antibiotic-induced conformational changes in ribosomal RNA: comparing aminoglycoside binding to prokaryotic and eukaryotic ribosomal RNA sequences, *J. Am. Chem. Soc. 126*, 3447–3453.
16. Shandrick, S., Zhao, Q., Han, Q., Ayida, B. K., Takahashi, M., Winters, G. C., Simonsen, K. B., Vourloumis, D., and Hermann, T. (2004) Monitoring molecular recognition of the ribosomal decoding site, *Angew. Chem., Int. Ed. Engl. 43*, 3177–3182.
17. Thomas, J. R., Liu, X., and Hergenrother, P. J. (2006) Biochemical and thermodynamic characterization of compounds that bind to RNA hairpin loops: toward an understanding of selectivity, *Biochemistry 45*, 10928–10938.
18. Thomas, J. R., Liu, X., and Hergenrother, P. J. (2005) Size-specific ligands for RNA hairpin loops, *J. Am. Chem. Soc. 127*, 12434–12435.
19. Thomas, J. R., DeNap, J. C., Wong, M. L., and Hergenrother, P. J. (2005) The relationship between aminoglycosides' RNA binding proclivity and their antiplasmid effect on an IncB plasmid combating drug-resistant bacteria: small molecule mimics of plasmid incompatibility as antiplasmid compounds, *Biochemistry 44*, 6800–6808.
20. Denap, J. C., Thomas, J. R., Musk, D. J., and Hergenrother, P. J. (2004) Combating drug-resistant bacteria: small molecule mimics of plasmid incompatibility as antiplasmid compounds, *J. Am. Chem. Soc. 126*, 15402–15404.
21. Klug, S. J., and Famulok, M. (1994) All you wanted to know about SELEX, *Mol. Biol. Rep. 20*, 97–107.
22. Joyce, G. F. (1994) In vitro evolution of nucleic acids, *Curr. Opin. Struct. Biol. 4*, 331–336.
23. Griffey, R. H., Hofstadler, S. A., Sannes-Lowery, K. A., Ecker, D. J., and Crooke, S. T. (1999) Determinants of aminoglycoside-binding specificity for rRNA by using mass spectrometry, *Proc. Natl. Acad. Sci. U.S.A. 96*, 10129–10133.
24. Swayze, E. E., Jefferson, E. A., Sannes-Lowery, K. A., Blyn, L. B., Risen, L. M., Arakawa, S., Osgood, S. A., Hofstadler, S. A., and Griffey, R. H. (2002) SAR by MS: a ligand based technique for drug lead discovery against structured RNA targets, *J. Med. Chem. 45*, 3816–3819.
25. He, Y., Yang, J., Wu, B., Robinson, D., Sprankle, K., Kung, P. P., Lowery, K., Mohan, V., Hofstadler, S., Swayze, E. E., and Griffey, R. (2004) Synthesis and evaluation of novel bacterial rRNA-binding benzimidazoles by mass spectrometry, *Bioorg. Med. Chem. Lett. 14*, 695–699.
26. Seth, P. P., Miyaji, A., Jefferson, E. A., Sannes-Lowery, K. A., Osgood, S. A., Propp, S. S., Ranken, R., Massire, C., Sampath, R., Ecker, D. J., Swayze, E. E., and Griffey, R. H. (2005) SAR by MS: discovery of a new class of RNA-binding small molecules for the hepatitis C virus: internal ribosome entry site IIA subdomain, *J. Med. Chem. 48*, 7099–7102.
27. Johnson, E. C., Feher, V. A., Peng, J. W., Moore, J. M., and Williamson, J. R. (2003) Application of NMR SHAPES screening to an RNA target, *J. Am. Chem. Soc. 125*, 15724–15725.

28. MacBeath, G., Koehler, A. N., and Schreiber, S. L. (1999) Printing small molecules as microarrays and detecting protein-ligand interactions en masse, *J. Am. Chem. Soc. 121*, 7967–7968.
29. Disney, M. D., and Seeberger, P. H. (2004) Aminoglycoside microarrays to explore interactions of antibiotics with RNAs and proteins, *Chemistry 10*, 3308–3314.
30. Ratner, D. M., Adams, E. W., Disney, M. D., and Seeberger, P. H. (2004) Tools for glycomics: mapping interactions of carbohydrates in biological systems, *ChemBioChem 5*, 1375–1383.
31. Afanassiev, V., Hanemann, V., and Wolfl, S. (2000) Preparation of DNA and protein microarrays on glass slides coated with an agarose film, *Nucleic Acids Res. 28*, E66.
32. Dufva, M., Petronis, S., Jensen, L. B., Krag, C., and Christensen, C. B. (2004) Characterization of an inexpensive, nontoxic, and highly sensitive microarray substrate, *Biotechniques 37*, 286–292294, 296.
33. Barrett, O. J., Childs, J. L., and Disney, M. D. (2006) Chemical microarrays to identify ligands that bind pathogenic cells, *ChemBioChem 7*, 1882–1885.
34. Bevilacqua, J. M., and Bevilacqua, P. C. (1998) Thermodynamic analysis of an RNA combinatorial library contained in a short hairpin, *Biochemistry 37*, 15877–15884.
35. Lato, S. M., and Ellington, A. D. (1996) Screening chemical libraries for nucleic-acid-binding drugs by in vitro selection: a test case with lividomycin, *Mol. Diversity 2*, 103–110.
36. Carlson, C. B., Vuyisich, M., Gooch, B. D., and Beal, P. A. (2003) Preferred RNA binding sites for a threading intercalator revealed by in vitro evolution, *Chem. Biol. 10*, 663–672.
37. Chan, T. R., Hilgraf, R., Sharpless, K. B., and Fokin, V. V. (2004) Polytriazoles as copper(I)-stabilizing ligands in catalysis, *Org. Lett. 6*, 2853–2855.
38. Kolb, H. C., and Sharpless, K. B. (2003) The growing impact of click chemistry on drug discovery, *Drug Discovery Today 8*, 1128–1137.
39. Kolb, H. C., Finn, M. G., and Sharpless, K. B. (2001) Click Chemistry: Diverse Chemical Function from a Few Good Reactions, *Angew. Chem., Int. Ed. Engl. 40*, 2004–2021.
40. Disney, M. D., and Childs-Disney, J. L. (2007) Using Selection to Identify and Chemical Microarray to Study the RNA Internal Loops Recognized by 6′-N-Acylated Kanamycin A, *ChemBioChem 8*, 649–656.
41. Yoshizawa, S., Fourmy, D., Eason, R. G., and Puglisi, J. D. (2002) Sequence-specific recognition of the major groove of RNA by deoxystreptamine, *Biochemistry 41*, 6263–6270.
42. Kirk, S. R., and Tor, Y. (1999) tRNA(Phe) binds aminoglycoside antibiotics, *Bioorg. Med. Chem. 7*, 1979–1991.
43. Cho, J., and Rando, R. R. (2000) Specific binding of Hoechst 33258 to site 1 thymidylate synthase mRNA aminoglycoside antibiotics are able to specifically bind the 5′-untranslated region of thymidylate synthase messenger RNA, *Nucleic Acids Res. 28*, 2158–2163.
44. Harada, K., and Frankel, A. D. (1999) Screening RNA-binding libraries using a bacterial transcription antitermination assay, *Methods Mol. Biol. 118*, 177–187.
45. Wu, M., and Turner, D. H. (1996) Solution structure of (rGCGGACGC)2 by two-dimensional NMR and the iterative relaxation matrix approach, *Biochemistry 35*, 9677–9689.
46. SantaLucia, J., Jr., and Turner, D. H. (1993) Structure of (rGGCGAGCC)2 in solution from NMR and restrained molecular dynamics, *Biochemistry 32*, 12612–12623.
47. Llano-Sotelo, B., Azucena, E. F., Jr., Kotra, L. P., Mobashery, S., and Chow, C. S. (2002) Aminoglycosides modified by resistance enzymes display diminished binding to the bacterial ribosomal aminoacyl-tRNA site, *Chem. Biol. 9*, 455–463.
48. Mendonsa, S. D., and Bowser, M. T. (2004) In vitro evolution of functional DNA using capillary electrophoresis, *J. Am. Chem. Soc. 126*, 20–21.
49. Dervan, P. B. (2001) Molecular recognition of DNA by small molecules, *Bioorg. Med. Chem. 9*, 2215–2235.
50. Milligan, J. F., and Uhlenbeck, O. C. (1989) Synthesis of small RNAs using T7 RNA polymerase, *Methods Enzymol. 180*, 51–62.
51. Disney, M. D., Testa, S. M., and Turner, D. H. (2000) Targeting a *Pneumocystis carinii* group I intron with methylphosphonate oligonucleotides: backbone charge is not required for binding or reactivity, *Biochemistry 39*, 6991–7000.
52. Disney, M. D., and Barrett, O. J. (2007) An aminoglycoside microarray platform for directly monitoring and studying antibiotic resistance, *Biochemistry 40*, 11223–11230.